The Role of the Biofilm Matrix in Structural Development

N. G. Cogan*

James P. Keener†

*Mathematics Department Tulane University New Orleans, LA. 70118 e-mail: cogan@math.tulane.edu FAX: 504 865 5063

†Mathematics Department University of Utah 155 South 1400 East, JWB 233 Salt Lake City, Ut. 84112-0090 e-mail: keener@math.utah.edu

Abstract

Although the initiation, development and control of biofilms has been an area of experimental investigation for more than three decades, the role of extra-cellular polymeric substance (EPS) has not been well studied.

We present a mathematical description of the EPS matrix to study the development of heterogeneous biofilm morphology. In developing the model, we assume that the biofilm is a biological gel composed of EPS and water. The bacteria are enmeshed in the network and are the producers of the polymer. In response to external conditions, gels absorb or expel solvent causing swelling or contraction due to osmotic pressure gradients. The physical morphology of the biofilm depends on the temperature, solvent composition, pH and ionic concentrations through osmotic pressure. This gives a physically based mechanism for the redistribution of biomass within the biofilm.

Analysis of a reduced model indicates that biomass redistribution, through the mechanism of swelling, may induce the formation of isolated towers or mushroom clusters by spatial variation in EPS production which leads to gradients in osmotic pressure.

Keywords: biofilm, EPS, gel, model, viscoelasticity, osmotic pressure

1 Introduction

Biofilms are communities of microorganisms anchored to a surface (substratum) and each other by EPS. Biofilms have a major impact on industrial, medical and environmental processes. These impacts include higher costs for production and distribution of products, causes of infections, and corrosion of equipment. Although the presence of biofilms is often detrimental, they have been used as biobarriers to both contain and reduce waste contaminations [4].

The varied settings for biofilm formation, as well as several properties of biofilms, such as resistance to anti-microbial agents, have made biofilm research an active area in the past three decades. As more research is done, and more properties of biofilms are discovered, the research has become more fundamental. Mathematical models have become an important

tool for evaluating hypotheses as well as suggesting new experimental inquiries. The purpose of this paper is to propose a mathematical model that incorporates some of the physical processes that underlie the formation of biofilm structure.

There are several questions that are relevant to modeling the development of biofilms. For example, it is important to understand the mechanisms of EPS production, redistribution and degradation, the role of quorum sensing, and the production and redistribution of biomass. It is also important to ascertain which models are most relevant and how the biofilm rheology should be treated (i.e. as a viscous fluid, viscoelastic material, two-phase material etc.).

The focus of this paper is on the mechanism of biomass redistribution. The production and redistribution of biomass has been modeled in several investigations in the literature [5, 8, 15, 16, 21, 22, 23, 27, 28, 29]. Briefly, we describe several different approaches to biomass redistribution.

Wimpenny and Colasanti developed a cellular automaton (CA) model which employs rules to determine when and if an individual bacterium divides [29]. In this model, a bacterium divides only if there is an empty neighboring location and a sufficient amount of substrate in the empty location. Thus, the bacteria do not exert a force on their neighbors. Instead, once a bacterium is surrounded, it ceases to reproduce.

Picioreanu et. al. [22, 21], derived a hybrid discrete-continuum model in which the spreading of the biomass is determined by cellular automata rules. In [22], bacterial growth is modeled by Monod kinetics with decay. Once the density of biomass within a grid location reaches a maximal value, the biomass divides into two parts. One part stays in place, and the other part is placed into a randomly chosen adjacent empty grid location if one exists. If all the neighboring cells are occupied, one of the nearest neighbors is displaced and must search for a new empty cell. This process continues until an empty cell is found. Thus, when a cell which is embedded deep within the biomass divides it effectively 'pushes' its neighbors extending the biofilm region.

Kreft et. al. [15], modeled the bacteria within the biofilm as spherical cells in continuous space. Biomass was redistributed by 'shoving' of cells to minimize the overlap of the cells. Simulations were able to produce morphologies which concur generally with those found in

CA-type models discussed above.

Recent models introduced by Eberl [8, 7] separate the bulk fluid region from the biofilm region. Within the biofilm region, the dynamics of the biomass density are governed by a reaction-diffusion equation. The investigators assume that the diffusion coefficient for the biomass density is density dependent. The structure of the diffusion coefficient causes the biomass to diffuse only when the biomass reaches a sufficient density.

Finally, a model due to Dockery and Klapper [5] described the formation of physical heterogeneity based on the assumption that the biofilm is a viscous fluid immersed in a fluid of much less viscosity. In their model, biomass is redistributed by an internal pressure due to bacterial growth. This pressure forces the free-interface between the biofilm and the bulk fluid to move so that a uniform density of bacteria is maintained.

While each model assumes a different mechanism for biomass redistribution, each of these models predict that substrate limitation can induce physically heterogeneous biofilm structure. In the absence of empirical investigation, it is not clear how to judge the validity of the redistribution mechanisms in the models except from the structures that are formed. One goal of the model described in this paper is to describe the mechanism of redistribution from more fundamental assumptions.

To develop a model which includes both the chemical structure and the physics of the EPS more realistically, we assume that the biofilm is a biological gel consisting of networked polymer (EPS) and fluid solvent (water). We assume that the primary forces which induce gel motion are applied to the fluid solvent and the EPS. This provides a mechanism of biomass redistribution through the swelling of the EPS and the viscoelastic constitutive relationships.

The network can be composed of several different polymers which may be hydrophilic or hydrophobic [30]. The polymer network can be formed by bonds or physical entanglement. In response to external conditions gel networks absorb or expel solvent causing swelling or contraction respectively. Thus the structure of the gel depends on the temperature, solvent composition, pH and ionic concentrations. The chemical potential that is responsible for the swelling properties of the gel is referred to as osmotic or swelling pressure.

A change in the external environment, for example, the addition of sodium ions, can

cause the gel to absorb more solvent and swell. However, if a cross-linking agent, such as calcium ions, is added to the solvent, polymers may be pulled together at cross-linking sites causing the gel to contract. In this way swelling decreases the volume fraction of the network and increases the volume occupied by the gel and contraction increases the network volume fraction decreasing the volume occupied by the gel. Thus the structure of the polymers and the ionic environment must be accounted for to predict the dynamic behavior of a gel.

Swelling and deswelling is a basic property of gels [20] and has been demonstrated in biofilm experiments [9, 10, 14]. The model presented below includes a redistribution mechanism that is based on the chemical structure of the EPS network and allows for swelling and deswelling of the biofilm gel. In particular, we model the biofilm as a hydrogel incorporating production of the polymer matrix. The model is analysed on the time scale of growth which is longer than the relaxation time scale, hence we include only Newtonian, viscous forces in the linear and nonlinear analysis.

2 Model Description

In this section we derive a model of biofilm growth and development which includes the main biological processes of bacterial growth and EPS production. The model assumes that biofilms consist of two immiscible materials, polymer network and fluid solvent. The model consists of equations of motion for the polymer and solvent material as well as the volume fraction of the polymer network, concentration of bacteria and the concentration of substrate.

The model has similarities with several models in the literature [11, 26, 19, 31] in which the dynamics of sea urchin eggs, hydrogels, tumors and hydrogels extruded by *Myxobacteria* are described. The treatment of the osmotic pressure and the network stresses are different in the present study. In particular, the osmotic pressure is taken from Flory-Huggins theory rather than qualitatively modeled as in [11, 26, 19]. Also the physical forces due to deformation of the matrix is separated from the chemical forces due to osmotic pressure.

We consider a region of space that contains networked polymer, solvent, substrate and bacteria. The network is assumed to act as a constant density, viscoelastic material and the solvent acts as a Newtonian fluid of much less viscosity than the networked material.

The substrate and the bacteria are assumed to be of negligible volume so that the volume fraction of network, θ_n, and the volume fraction of solvent, θ_s, sum to one. This assumption is not universally valid. The volume occupied by the bacteria in biofilms formed by mucoid strains of *Pseudomonas aeruginosa* can be as little as 1%, while the volume occupied by other strains of bacteria can be as high as 50%. Thus, our model is not valid if the bacteria comprise a substantial volume fraction.

We assume that there are four forces that act on the network. The first are surface forces that are described mathematically as $\nabla \cdot (\theta_n \sigma_n)$, where σ_n is the network stress tensor. We assume that there are two kinds of stress within the gel, a Newtonian stress that is related to the strain rate and a non-Newtonian stress that includes elastic stress. Hence we separate the stress as $\sigma_n = \sigma_v + \sigma_e$, where σ_v is the viscous stress and σ_e is the elastic stress. Constitutive relations must be specified to completely determine these. Typically the viscous stress is assumed to be proportional to the velocity gradient as $\sigma_v = \frac{1}{2}(\nabla \vec{U_n} + \nabla \vec{U_n}^T)$. Another approach is to describe the total stress in terms of the deformation gradient and the velocity gradient. See [3, 18] for a review of several constitutive relations used to specify the elastic stress.

The second force we include is frictional drag generated by network material interacting with fluid material. This term vanishes if the network and fluid velocities are equal or if either of the volume fractions of network and fluid are zero. We model the frictional force by $h_f \theta_n \theta_s (\vec{U_n} - \vec{U_s})$, where $\vec{U_s}$, $\vec{U_n}$, h_f denote the solvent velocity, network and the constant coefficient of friction, respectively.

The third force is induced by the colligative properties of the gel. To model this force, we assume that there exists an osmotic pressure, $\Psi(\theta_n)$, gradients of which create force on the polymers due to chemical environment. Inclusion of this component is based on the observations discussed above. This pressure has also been theoretically derived for two-phase fluid models as the "inter-phase pressure" [6].

To model this term, we use Flory-Huggins theory [17, 20], in which the osmotic pressure is given by

$$\Psi = -\frac{k_B T}{v_1}\left(\ln(1-\theta_n) + (1-\frac{1}{m})\theta_n + \chi_1 \theta_n^2\right), \quad (1)$$

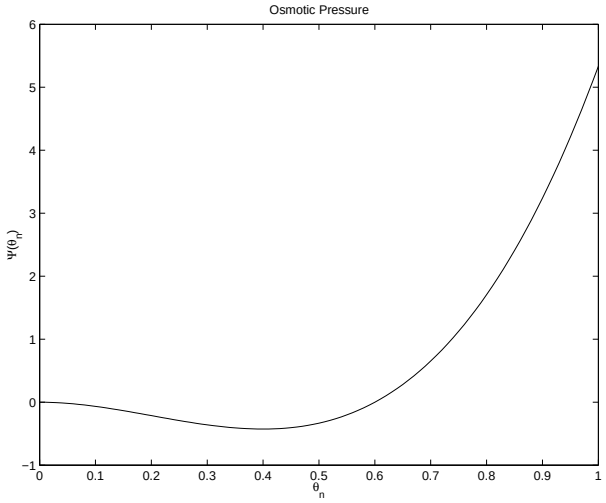

Figure 1: Swelling pressure for parameters $\frac{k_B T}{v_1} = 40\text{pN/nm}^2$, $v_1 = .1\text{nm}^3$, $\chi_1 = .7$.

where m is the ratio of solvent volume to polymer volume, χ_1 is the Flory interaction parameter which measures the strength of attraction between the polymer chains, k_B is Boltzmann's constant, T is the temperature. The parameter v_1 is the volume occupied by one monomer of the network constituent. Because m is large, we approximate this with

$$\Psi = -\frac{k_B T}{v_1}\left(\ln(1-\theta_n) + \theta_n + \chi_1 \theta_n^2\right). \tag{2}$$

This term is often rewritten by expanding $\ln(1-\theta_n)$ in a Taylor's series about $\theta_n = 0$. Retaining the terms up to θ_n^3, we find

$$\begin{aligned} \Psi &= \frac{k_B T}{v_1}\left((\frac{1}{2} - \chi_1)\theta_n^2 + \frac{\theta_n^3}{3}\right) \\ &= \frac{k_B T}{3v_1}\theta_n^2\left(\theta_n - 3(\chi_1 - \frac{1}{2})\right). \end{aligned} \tag{3}$$

Although this expansion is valid for θ_n near zero, it is often used for $0 < \theta_n < 1$ [20].

A plot of Ψ from equation 3 is given in Figure 1.

Because there is little experimental data concerning osmotic pressure in biofilms, it is difficult to find several specific parameters such as v_1 and χ_1; therefore we take the qualitative, cubic form as our simplified model of osmotic pressure. Specifically the osmotic

pressure, equation (3) is written $\Psi(\theta_n) = \xi_{os}\theta_n^2(\theta_n - \theta_{ref})$, where θ_{ref} is a reference volume fraction. Therefore the swelling pressure is zero if $\theta_n = 0$ or $\theta_n = \theta_{ref}$. This treats all the water in the biofilm as solvent, neglecting the water contained in the bacteria. Numerical experiments done with other reference volume fractions do not differ qualitatively. All effects from the ionic environment, polymer structure, and solvent concentration are lumped into the parameter ξ_{os}.

The final force that is included is hydrostatic pressure. We define P to be the total hydrostatic pressure that acts on the entire volume. Therefore the amount of force due to pressure that acts on network is $\theta_n \nabla P$.

Combining these terms and ignoring inertial effects, we obtain the momentum balance equation,

$$\begin{aligned} \eta_n \nabla \cdot (\theta_n(\sigma_v + \sigma_e)) - h_f \theta_n \theta_s (\vec{U}_n - \vec{U}_s) & \\ -\nabla \Psi(\theta_n) - \theta_n \nabla P &= 0. \end{aligned} \tag{4}$$

The equation that governs the solvent momentum is derived in a similar manner. The first force is the stress on the solvent which is given mathematically as $\nabla \cdot (\theta_s \sigma_s)$ for the solvent stress tensor σ_s. Since the solvent is assumed to be a Newtonian fluid, σ_s contains only viscous stresses, and is therefore given by $\sigma_s = \frac{1}{2}(\nabla \vec{U}_s + \nabla \vec{U}_s^{\,T})$. The second force is the force due to interaction between the network and fluid which is the same term as appears in the network equation, Equation 4, with the opposite sign. The final force is the fluid pressure applied to the solvent fluid.

Combining these terms and assuming that the solvent is in force balance, we obtain the momentum balance equation

$$\eta_s \nabla \cdot (\frac{\theta_s}{2}(\nabla \vec{U}_s + \nabla \vec{U}_s^{\,T})) + h_f \theta_n \theta_s (\vec{U}_n - \vec{U}_s) - \theta_s \nabla P = 0. \tag{5}$$

The equation describing the network redistribution is derived by applying the principle of conservation of mass. Since the network moves with a velocity $\vec{U}_n$, the flux into an infinitesimal volume is given by $\nabla \cdot (\theta_n \vec{U}_n)$. The production of the network is denoted g_n

and depends on bacterial concentration, substrate concentration and the volume fraction of network. Putting these terms together we have that the redistribution of network material is governed by

$$\frac{\partial}{\partial t}\theta_n + \nabla \cdot (\theta_n \vec{U}_n) = g_n. \tag{6}$$

A similar equation describes the conservation of solvent, namely

$$\frac{\partial}{\partial t}\theta_s + \nabla \cdot (\theta_s \vec{U}_s) = 0. \tag{7}$$

Assuming that $\theta_n + \theta_s = 1$, we combine (7) and (6) to conclude that the divergence of the average flow, $\theta_n \vec{U}_n + \theta_s \vec{U}_s$, is constrained to balance the production of network

$$\nabla \cdot (\theta_n \vec{U}_n + \theta_s \vec{U}_s) = g_n. \tag{8}$$

We now consider the principle of conservation of mass applied to the bacterial concentration, B. The bacteria are advected by the network, since they are assumed to be physically entangled within the network. The bacteria also reproduce with growth g_b which depends on substrate concentration and bacterial concentration. Combining these terms, the concentration of bacteria is governed by

$$\frac{\partial}{\partial t}B + \nabla \cdot (B \vec{U}_n) = g_b. \tag{9}$$

The concentration of substrate, c, is changed by the amount of material moving in and out of a control volume. Since the substrate is dissolved in the solvent there is flux due to solvent motion as well as molecular diffusion. The flux due to solvent motion is proportional to the velocity of the solvent, the concentration of substrate and the volume fraction of solvent. If the volume fraction or velocity of solvent become zero there is no transport. The flux of substrate concentration due to diffusion is assumed to be proportional to the gradient of the substrate concentration, with constant of proportionality D. The diffusive flux is assumed to be scaled by the volume fraction of solvent, therefore, the change in concentration due

to molecular motion is given by $D\nabla \cdot (\theta_s \nabla c)$. The final component of the equation, $-g_c$, describes the utilization of the substrate by bacteria where the minus sign indicates that substrate is consumed rather than produced. We then have the equation

$$\frac{\partial}{\partial t}(\theta_s c) + \nabla \cdot (c\vec{U}_s \theta_s - D\theta_s \nabla c) \quad = \quad -g_c, \tag{10}$$

that governs the concentration of substrate at each point in time and space.

Equations 4, 5, 6, 9 and 10 give the governing equations for a growing bio-gel.

To describe the production and redistribution of EPS, a form for the growth function, g_n, must be specified. In general, the production of EPS is complicated and depends on the bacterial concentration, substrate concentration and network volume fraction. To simplify the analysis that follows, we assume that the network density is proportional to the bacterial concentration. The production of EPS is often modeled using a term that is proportional to the bacterial growth and a term that is independent of the growth (Luedeking-Piret equation [13]).

When the bacteria are undergoing exponential growth (i.e. when the growth rate is proportional to concentration of bacteria), assuming that the network density is proportional to the bacterial concentration allows us to eliminate the equation determining the bacterial concentration, as long as the growth independent rate is negligible. This is a naive assumption. However, in this study, the focus is on the qualitative effect of EPS production, rather than on quantitative study of various production models. We argue that assuming that the bacteria are uniformly distributed throughout the EPS matrix and that production of EPS is proportional to the bacterial growth rate leads to qualitatively similar phenomena, namely, EPS production is high in the presence of abundant substrate. Although there are several experimental observations that cannot be addressed by the reduced model, such as clonal growth, the model is sufficiently complicated as to warrant this reduction. We assume that the kinetics of network production is modeled by Monod kinetics , i.e., $g_n = \epsilon \mu \theta_n \frac{c}{K_c + c}$, where K_c is the half-saturation constant and μ is the maximum production rate. Hence the growth rate of network is a saturating function of the substrate concentration.

The production is scaled by ϵ to reflect the fact that production is slow on the time

Figure 2: Sketch of the computational region. The domain is separted into two subdomains, Ω (biofilm region) and $\bar{\Omega}$ (Bulk Fluid Region).

scale of network motion. When the concentration of substrate in the bulk fluid is small, the biofilm is in a substrate limited environment. In this regime, g_n may be approximated by $g_n = \epsilon A \theta_n c$, where $A = \frac{\mu}{K_c}$.

Because diffusion of substrate is on the order of seconds and the time scale of network motion is on the order of hours, the substrate is assumed to be in quasi-steady-state. The consumption of substrate is related to the growth rate of network, $g_c = \theta_n A c$. The substrate equation becomes

$$D\nabla \cdot ((1-\theta_n)\nabla c) \quad = \quad A\theta_n c. \tag{11}$$

3 Simplifications and Analysis

We suppose that a region of space is separated into two sub-regions, one region, Ω, is occupied by growing biofilm while the second region, $\bar{\Omega}$, contains only water (see figure 3). The substrate diffuses passively in $\bar{\Omega}$ and is introduced into the system far from Ω.

If the interface between Ω and $\bar{\Omega}$ is flat and the bacterial concentration depends only on the depth, then the problem reduces to a one-dimensional spatial problem and production of polymer within Ω causes the region to grow uniformly. If the interface is not uniform, the growth is not uniform, since substrate diffusion into the biofilm allows the bacteria in the peaks of the perturbed region easier access to substrate than those in the troughs. Hence, higher growth rates obtain within the peaks, which creates larger osmotic forces there. This, in turn, causes the network to have larger velocity at the peaks than in the troughs reinforcing

the perturbation, in the absence of surface effects such as surface tension or diffusion of the polymer.

Because the full system of equations is complicated, we search for reasonable simplifying assumptions about the physical parameters of the system. The biofilm network and bulk fluid velocities are coupled only through the frictional terms and since the polymers that comprise most of the biofilm are of relatively low volume fraction [1, 14] and the solvent flow within the network is slow, it seems reasonable that the force due to friction is small; therefore we take $h_f = 0$. Since the bulk fluid and network momentum equations are uncoupled in the absence of friction, the fluid velocity is taken to be zero without affecting the network motion. Equation 5 implies that $\nabla P = 0$ under the assumption $\vec{U_s} = 0$. The reduced network momentum equation becomes

$$\eta_n \nabla \cdot (\theta_n(\sigma_v + \sigma_e)) - \nabla \Psi(\theta_n) = 0. \tag{12}$$

The most significant time-scale is determined by the growth of the biofilm region (hours - days) which is long compared to the time scale of polymer relaxation (seconds). Therefore we assume that the network has sufficient time to relax and the stress is dominated by the viscous component. Under this assumption the stress is related to the velocity gradient as $\sigma_n = \frac{1}{2}(\nabla \vec{U_n} + \nabla \vec{U_n}^T)$.

The interface between Ω and $\bar{\Omega}$ is denoted $\vec{\Gamma}(\vec{x}, t)$ and constitutes one of the boundaries of the biofilm region. As the network is produced and moves in time and space, this boundary changes. That is, this is a free boundary. For consistency, the normal component of the interface velocity must match the normal component of the network velocity. The consistency condition is described mathematically by

$$\frac{\partial \vec{\Gamma}}{\partial t} \cdot \vec{n} = \vec{U} \cdot \vec{n}, \tag{13}$$

where $\vec{n}$ is the unit vector normal to the interface.

There is no normal stress on the network at the interface, i.e.,

$$(\eta_n \frac{\theta_n}{2}(\nabla \vec{U_n} + \nabla \vec{U_n^T}) - \Psi(\theta_n) I + \kappa \nabla \cdot \vec{n} I) \cdot \vec{n} = 0 \tag{14}$$

on $\vec{\Gamma}$. The term $\nabla \cdot \vec{n} I$ represents the stress due to surface tension and is assumed to be proportional to the curvature of the interface with constant of proportionality κ (N/m).

Equations 6, 11, 12, 13 and the stress-free condition 14 determine the network velocity, volume fraction of network, substrate concentration and boundary motion for the reduced system.

We use two methods to analyse the growth of the biofilm domain. We first study the linear stability of the flat interface. Then, to determine the nonlinear behavior, we simulate the full set of equations numerically.

Because this is a free-boundary problem, linear stability analysis is not trivial. We restrict ourselves to two spatial dimensions and assume that the interface is given by $\vec{\Gamma} = (x, \gamma(x,t))$, where the interface is located far from the substratum. The assumption that γ is a function of x precludes the formation of 'mushrooms' in the linear analysis. The initial, unperturbed boundary lies on the x-axis, and the unperturbed domain is the lower-half plane and the domain moves as a result of production of network. The variables θ_n, $\vec{U}$ and c are assumed to be periodic in x, with period L. Both the substrate concentration and the velocity decay as $y \to -\infty$. We assume that the bulk liquid is well mixed so that, at the interface, the substrate concentration is c_{max}.

The biofilm region is determined by the network volume fraction, θ_n, and therefore changes as the network is produced and is redistributed. We make a time-dependent change of coordinates which fixes the domain on the lower-half plane in the new coordinates. This maps the physical domain into a fixed coordinate system, $s \in (0,1)$, $h \in (-\infty, 0]$.

The new coordinate system is given by $s = x$, $h = y - \gamma(s,\tau)$, and $\tau = t$. The differential operators in h,s-coordinates are related to those in x,y-coordinates by

$$\begin{aligned} \frac{\partial}{\partial x} &= \frac{\partial}{\partial s} - \frac{\partial \gamma}{\partial s}\frac{\partial}{\partial h}, \\ \frac{\partial}{\partial y} &= \frac{\partial}{\partial h}, \\ \frac{\partial}{\partial t} &= \frac{\partial}{\partial \tau} - \frac{\partial \gamma}{\partial \tau}\frac{\partial}{\partial h}. \end{aligned}$$

In the new coordinate system, we are able to study the stability of the steady-state,

s-independent solution. The presence of the small parameter ϵ is exploited, by solving the s and τ independent problem in an asymptotic sense. That is, we assume a power series representation of the solutions and find the leading order approximations to network volume fraction and network horizontal and vertical velocities, denoted θ_0, v_0 and w_0, respectively. The biofilm is growing and we expect the interface to move at a constant rate to balance the growth, thus we seek solutions for which θ_n is constant in space and time to leading order. Since the growth is $\mathcal{O}(\epsilon)$, we expect the interface motion to be of the same order, that is $\frac{\partial \gamma}{\partial \tau} = \epsilon k$.

The solutions to the leading order equations are

$$\begin{aligned} w_0 &= 0, \\ \theta_0 &= \hat{\theta}, \\ c_0 &= c_{max} e^{\mathrm{r}\sqrt{\frac{\hat{\theta}}{D(1-\hat{\theta})}}h}, \end{aligned}$$

where $\hat{\theta}$ is a constant such that $\Psi(\hat{\theta}) = 0$.

The leading order corrections can be found by considering the $\mathcal{O}(\epsilon)$ equations. We find that the leading order correction to the vertical component of the network velocity is

$$w_1 = \frac{c_{max}}{\sqrt{\frac{\hat{\theta}}{D(1-\hat{\theta})}}} e^{\mathrm{r}\sqrt{\frac{\hat{\theta}}{D(1-\hat{\theta})}}h} + K,$$

and since w_1 must vanish at $h = -\infty$, $K = 0$. The order ϵ consistency condition reduces to $k_0 = w_1|_{h=0} = c_{max}\sqrt{\frac{D(1-\hat{\theta})}{\hat{\theta}}}$. Therefore the boundary motion is proportional to the substrate load, as one might expect.

We linearize Equations 12, 6 and 11 about the steady-state solution by assuming that the interface is perturbed by a small amplitude periodic function. The consistency condition, Equation 13, relates the motion of the interface to the frequency of the perturbation. This relationship is referred to as the dispersion curve [2]. Surface tension has the effect of penalizing the oscillatory interfaces, assuring that the higher mode perturbations are damped out.

The nonlinear (numerical) analysis is also complicated by the free boundary. To make the problem easier to simulate numerically, we assume that the network diffuses due to molecular motion, with diffusion coefficient δ. This smooths out the sharp boundary and allows us to extend the computational domain to include $\bar{\Omega}$. The location of the biofilm/bulk water interface is indicated by a rapid transition in network volume fraction. This assumption is probably more realistic than the sharp interface assumption, since in experimental biofilms there is a 'mushy' zone where it is difficult to distinguish between the biofilm and the bulk fluid. Under these assumptions, the network equation used in the simulations becomes

$$\frac{\partial}{\partial t}\theta_n + \nabla \cdot (\theta_n \vec{U}_n) \quad = \quad \epsilon A \theta_n c + \delta \Delta \theta_n. \tag{15}$$

4 Results

The dispersion curve, which relates the growth rates, λ, to the perturbation frequency, α, is derived from the linear analysis. The effect of the surface tension is shown for varying proportionality constants κ in Figure 4. As expected, surface tension is a stabilizing force. We see that there is a mode which is maximally unstable, as well as a frequency above which the perturbations decay. This result is in qualitative agreement with the result from [5], although there is no additional surface tension needed in their model.

We use numerical simulations to explore the behavior beyond the linear regime. A description of the numerical scheme is given in Appendix A. Table I lists typical parameter values used for each of the simulations. These parameters are typical for a biofilm containing one species of bacteria and oxygen as the limiting substrate [24]. The domain size is 1mm $\times$ 1mm, with a grid of 100 $\times$ 100, thus the grid spacing is approximately 10μm. The coefficient of the osmotic pressure, ξ_{os}, is estimated by requiring that the velocity of the biofilm due to growth and redistribution is comparable to that of experimental biofilms.

In the first simulation the interface is perturbed by a single, low frequency perturbation which is enhanced by production and redistribution. After approximately 3.6 days, the original perturbation has been amplified as shown in Figure 6. The growth rate is shown in Figure 5, which indicates that the growth is concentrated at the peak of the perturbation.

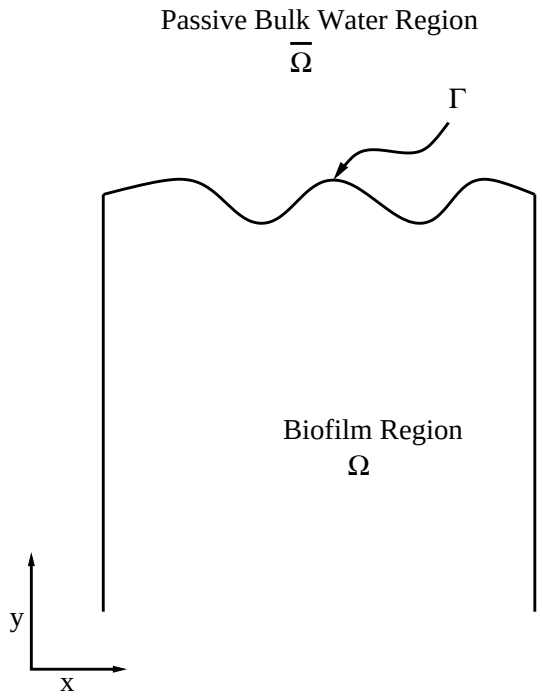

Figure 3: Sketch of the computational region. The two-dimensional domain.

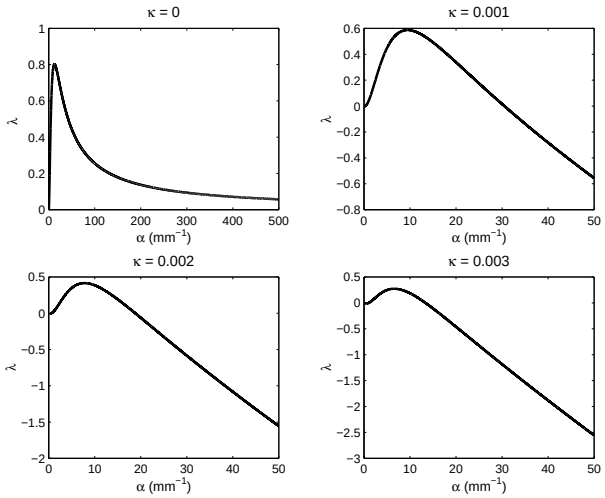

Figure 4: The dispersion curve for varying surface tensions, κ.

Symbol	Parameter	Value	Units	Source
D	Substrate Diffusion Coefficient	2.3×10^{-9}	$\mathrm{m^2 s^{-1}}$	[24]
μ	Max. Consumpt. Rate (Low)	2.3×10^{-4}	$\mathrm{kgm^{-3} s^{-1}}$	[24]
	(High)	1.4×10^{-3}	$\mathrm{kgm^{-3} s^{-1}}$	[24]
K_c	Half Saturation Constant	1×10^{-4}	$\mathrm{kgm^{-3}}$	[24]
δ	Network Diffusion Coefficient	3×10^{-8}	$\mathrm{m^2 s^{-1}}$	Assumed
c_{max}	Substrate Source Coefficient	1×10^{-3}	$\mathrm{kgm^{-3}}$	[24]
η_n	Dynamic Viscosity	4.3×10^{2}	$\mathrm{Ns/m^2}$	[12]
ξ_{os}	Osmotic Pressure Coefficient	4.3×10^{3}	$\mathrm{N/m^2}$	estimated

Table I: Parameter values used in the simulations

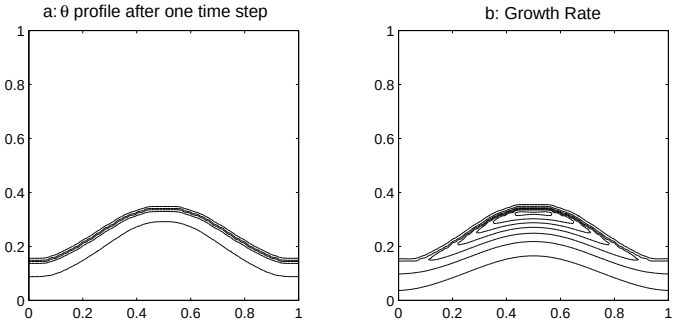

Figure 5: a.) Contour plot of the θ_n profile and b.) contours of differential growth rate after one time step. In regions of high growth rate, the local volume fraction of network increases increasing the osmotic pressure locally. The initial interface is highlighted and the parpamters are given in 4 with $\mu = 2.3 \times 10^{-4}$ $\mathrm{kgm^{-2} s^{-1}}$.

The interface in the next simulation is also perturbed by a single mode. The scale of the domain has been increased to 2mm $\times$ 2mm and the perturbation is chosen so that the peak is far from the boundary so that we see the 'mushrooming' behavior in Figure 7.

In regions of high production, the volume fraction of EPS exceeds the reference value θ_{ref}. Therefore the osmotic pressure is higher which leads to more displacement of biomass. Hence we expect that for higher production rate the formation of 'mushrooms' should be faster. To test this, the same initial condition as that in Figure 7 is used but a higher growth rate is assumed (see 4. We see a secondary instability as shown in Figure 8. The linear analysis shows that flat interfaces are unstable and the differential growth can reinforce perturbations. Therefore, if the 'mushroom' is sufficiently large there is a possibility of a second instability causing so-called tip-splitting [25].

Simulations with a higher frequency initial interface perturbation yield more 'mushroom-like' towers as shown in Figure 9.

The flat interface is stable to perturbations of high spatial frequency. The perturbations are overwhelmed by diffusion until there is a spatially uniform band of growth along the interface. Results for this simulation are shown in Figure 10.

One of the hypotheses concerning biofilm heterogeneity is that for low substrate load, there is a rougher biofilm since there is more competition for resource [21, 5, 8]. To test this hypothesis with our model we simulated a growing biofilm cluster for 50 hours using linear growth and consumption kinetics (first order kinetics). We then change from linear to saturated kinetics by assuming that $g_n = \epsilon\mu\theta_n$ in Equation 6 (zero order kinetics). In Figure 11, we see the irregular interface is smoothed out, since there is no longer differential growth. A comparison of the two regions, linear kinetics after 50 hours and saturated kinetics for the next 50 hours is shown in Figure 11. This agrees with conclusions from [5] and [21].

5 Conclusions

We have presented a model of biofilm growth that is based on the structure of the EPS. It is important to include EPS since the majority of the biomass of the biofilm consists of EPS and the polymer network endows biofilms with material properties that regulate its movement.

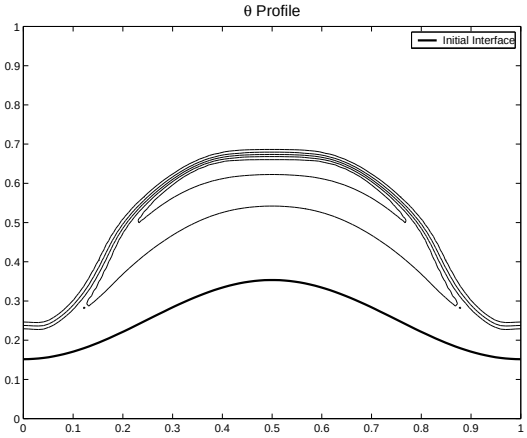

Figure 6: Contours of volume fraction of network showing the growth of the domain after 3.6 days. The initial interface and parameters are the same as in figure 5.

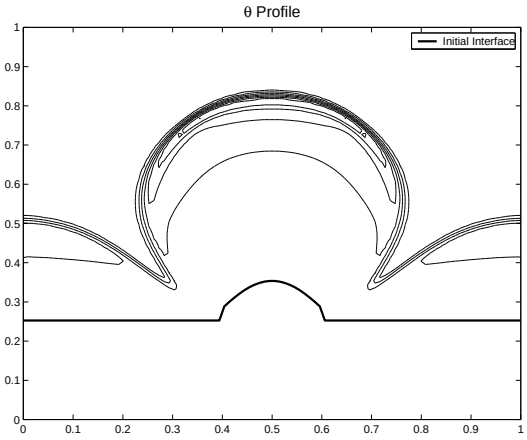

Figure 7: Contours of network volume fraction, showing the development of a mushroom-shaped tower after 3.6 days. The initial interface is localized in the center of the domain which is 2 mm $\times$ 2 mm. The growth rate is $\mu = 2.3 \times 10^{-4}$ kgm^{-2}s^{-1}.

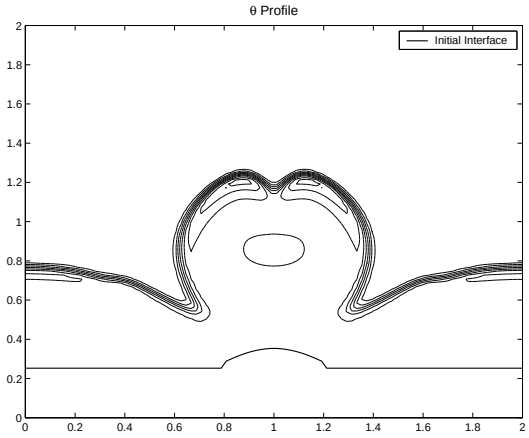

Figure 8: Contours of network volume fraction, showing the onset of a secondary instability after 3.6 days with a higher growth rate (i.e $\mu = 1.4 \times 10^{-3}$ kgm^{-2}s^{-1}. All other parpamters are listed in **??**

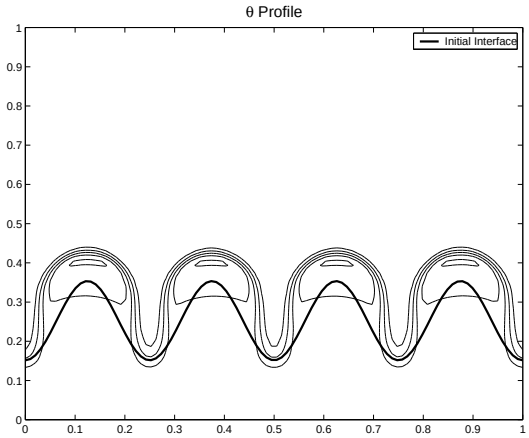

Figure 9: Contours of network volume fraction, showing the interaction between several towers after 3.6 days.

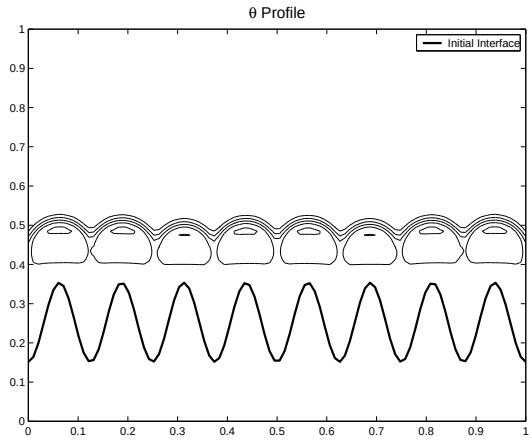

Figure 10: Contours of network volume fraction, showing the smoothing of the interface with a high mode perturbation after 3.6 days.

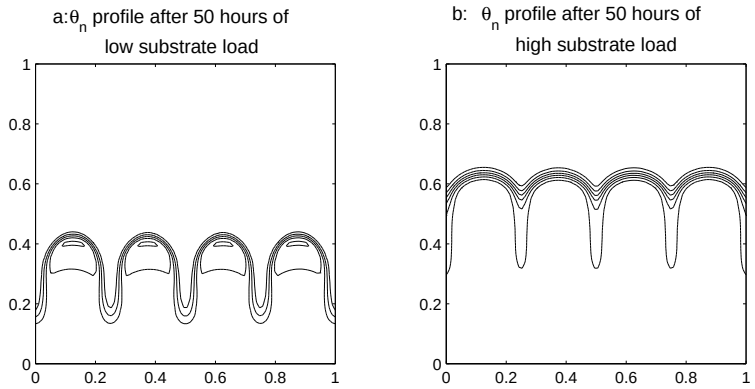

Figure 11: A comparison between the domain with a: linear kinetics and b: saturated kinetics. The figure on the left is the biofilm domain after 50 hours of growth with linear kinetics. The figure on the right is the continuation of the simulation with saturated kinetics. The towers formed in the first 50 hours are smoothed out and the amplitude of the interface is decreasing (i.e., stabilized).

In this model as polymer is produced by bacteria the osmotic pressure increases, causing the gel to swell and leading to the expansion of the biofilm region. Results from preliminary analysis of the simplified model indicates that the formation of towers and mushrooms may be due to the interaction between differential production and chemical properties of the EPS through the osmotic pressure. We have shown evidence from simulations that the formation of these heterogeneous structures depends on the substrate loading which is in agreement with several other models [5, 22, 21].

Numerical evidence of secondary instabilities was given. It has not been determined whether the full model has these instabilities; however, the mechanism which causes the development of heterogeneity seems quite robust to chagnes in paramters and initial interfaces. However, including the elastic stress in the network may alter this behavior.

This work was supported by the NSF-FRG grant #DMS 0139926

A Numerical Techniques

We describe the discretization of the two-dimensional equations which describe the substrate distribution, momentum and redistribution of a growing gel. These equations are defined on the interior of a two-dimensional domain which is periodic in the horizontal direction and is bounded below by the substratum and above by a free-boundary defined by the interface between the biofilm and the bulk fluid. The equations have been simplified by assuming no frictional interaction between the network and the solvent thus allowing us to set the solvent velocity to zero. The network is also assumed to be in force balance, eliminating the inertial terms that appear on the left-hand-side of Equation 4. The motion of the free-boundary is determined by a consistency condition which requires the motion of the interface to be consistent with the motion of the network. The reduced equations are

$$\eta_n \nabla \cdot (\frac{\theta_n}{2}(\nabla \vec{U}_n + \nabla \vec{U}_n{}^T)) - \nabla \Psi(\theta_n) = 0, \tag{16}$$

$$\frac{\partial}{\partial t}\theta_n + \nabla \cdot (\theta_n \vec{U}_n) = g_n, \tag{17}$$

$$\nabla \cdot (D(1-\theta_n)\nabla c) = g_c, \tag{18}$$

$$\frac{\partial \vec{\Gamma}}{\partial t} \cdot \vec{n} = \vec{U} \cdot \vec{n}. \tag{19}$$

To solve these equations, we include a small amount of diffusion to the network redistribution equation, 17, and extend the domains of these equations to the entire region Ω. This technique smooths out the interface, hence the interface equation 19 is not used. Instead the motion of the boundary is implicit in the solution of the network conservation equation 17, where the sharp boundary is characterized by a rapid change in the network volume fraction. Mathematically we replace Equation 17 with

$$\frac{\partial}{\partial t}\theta_n + \nabla \cdot (\theta_n \vec{U}_n) = g_n + \delta \Delta \theta_n. \tag{20}$$

Because the network volume fraction θ_n is close to zero in the bulk fluid region, the operator defined by the first term in Equation 16 is singular. To numerically approximate the solutions, we include a small amount of network in the bulk region when solving this

equation. That is Equation 16 is approximated by

$$\eta_n \nabla \cdot (\frac{\theta_{\delta n}}{2}(\nabla \vec{U}_n + \nabla \vec{U}_n{}^T)) - \nabla \Psi(\theta_{\delta n}) \;\; = \;\; 0, \tag{21}$$

where

$$\theta_{\delta n} = \begin{cases} \theta_n(x,y,t) & if (x,y) \in \Omega \\ \theta_n(x,y,t) + r & if (x,y) \in \bar{\Omega} \end{cases}$$

We also separate the horizontal and vertical components of the first term of Equation 21, $\nabla \cdot (\frac{\theta_n}{2}(\nabla \vec{U} + \nabla \vec{U}^T))$, into two pieces so that one part is the more typical operator $\nabla \cdot (\theta_n \nabla V)$ and the remaining part is moved to the right-hand-side and used as data for the time iteration of the system. This ensures that the matrix equation obtained by discretizing the problem is symmetric and that the left-hand-sides of the component equations determine either the vertical or horizontal components of the velocity field.

The horizontal component of the velocity equation becomes

$$\frac{\partial}{\partial x}(\theta_{\delta n}\frac{\partial V}{\partial x}) + \frac{\partial}{\partial y}(\frac{\theta_{\delta n}}{2}(\frac{\partial W}{\partial x} + \frac{\partial V}{\partial y}) \;\; = \;\; \frac{\partial \Psi(\theta_{\delta n})}{\partial x}$$

or

$$\begin{aligned} \frac{\partial}{\partial x}(\theta_{\delta n}\frac{\partial V}{\partial x}) + \frac{\partial}{\partial y}(\theta_{\delta n}\frac{\partial V}{\partial y}) \;\; = \;\; & \frac{\partial}{\partial y}(\frac{\theta_{\delta n}}{2}\frac{\partial V}{\partial y}) - \frac{\partial}{\partial y}(\frac{\theta_{\delta n}}{2}\frac{\partial W}{\partial x}) \\ & + \frac{\partial \Psi(\theta_{\delta n})}{\partial x}, \end{aligned} \tag{22}$$

and the vertical component of the velocity is governed by

$$\frac{\partial}{\partial x}(\frac{\theta_{\delta n}}{2}(\frac{\partial W}{\partial x} + \frac{\partial V}{\partial y}) + \frac{\partial}{\partial y}(\theta_{\delta n}\frac{\partial W}{\partial y}) \;\; = \;\; \frac{\partial \Psi(\theta_{\delta n})}{\partial y}$$

or

$$\begin{aligned} \frac{\partial}{\partial x}(\theta_{\delta n}\frac{\partial W}{\partial x}) + \frac{\partial}{\partial y}(\theta_{\delta n}\frac{\partial W}{\partial y}) \;\; = \;\; & \frac{\partial}{\partial x}(\frac{\theta_{\delta n}}{2}\frac{\partial W}{\partial x}) - \frac{\partial}{\partial x}(\frac{\theta_{\delta n}}{2}\frac{\partial V}{\partial y}) \\ & + \frac{\partial \Psi(\theta_{\delta n})}{\partial y}. \end{aligned} \tag{23}$$

We now have four coupled equations to solve numerically: Equations 20, 22, 23 and 18. The boundary conditions for all variables are assumed to be periodic in x. The network volume fraction, $\theta_{\delta n}$ satisfies Neumann boundary conditions on the bottom boundary, Σ_1, and the top boundary, Σ_2. The substrate satisfies a Neumann boundary condition on Σ_1 and Dirichlet boundary conditions at the top with $c = c_{max}$ on Σ_2. The components of the network velocity are assumed to be zero on Σ_1 and Σ_2.

We begin by initializing the biofilm region by setting

$$\theta_{\delta n} = \begin{cases} \theta_{ref} & \text{if}(x,y) \in \Omega \\ 0 & \text{if}(x,y) \in \bar{\Omega} \end{cases}$$

for a given interface Γ. The substrate and network velocities are initially zero.

To define the discretized equations we define the domain to be a rectangle $L_1 \times L_2$ with an associated $N \times M$ mesh with spacing $dx = \frac{L_1}{N}$ and $dy = \frac{L_2}{M}$. Thus the continuous variables $\vec{U} = (V(x,y,t), W(x,y,t))$, $\theta(x,y,t)$ and $c(x,y,t)$ are approximated by the discrete variables $\mathbf{V}^k_{i,k} = V(x_i, y_j, t_k)$, $\mathbf{W}^k_{i,k} = W(x_i, y_j, t_k)$, $\theta_{\delta \mathbf{n}}{}^k_{i,j} = \theta_{\delta n}(x_i, y_j, t_k)$, $\mathbf{c}^k_{i,j} = c(x_i, y_j, t_k)$, where $x_i = idx$, $y_j = jdy$, $t_k = kdt$ for $i = 0...N$, $j = 0...M$, and $k = 0...T_{max}$. We also define the centered difference operators

$$\begin{aligned} \delta_x \phi(x,y,t) &= \phi(x+dx,y,t) - \phi(x-dx,y,t), \\ \delta_y \phi(x,y,t) &= \phi(x,y+dy,t) - \phi(x,y-dy,t). \end{aligned}$$

With this notation in hand, we now define the discrete approximation to the continuous equations 20, 22, 23 and 18. The discretized version of network conservation is

$$\begin{aligned} \frac{\theta_{\delta \mathbf{n}}{}^{k+1}_{i,j} - \theta_{\delta \mathbf{n}}{}^{k}_{i,j}}{dt} - \left(\frac{\delta_x^2 \theta_{\delta \mathbf{n}}{}^{k+1}_{i,j}}{dx^2} + \frac{\delta_y^2 \theta_{\delta \mathbf{n}}{}^{k+1}_{i,j}}{dy^2}\right) &= g_n(\theta_{\delta \mathbf{n}}{}^{k}_{i,j}, \mathbf{c}^k_{i,j}) \\ &\quad -\delta_x(\theta_{\delta \mathbf{n}}{}^{k}_{i,j} \mathbf{V}^k_{i,j}) - \delta_y(\theta_{\delta \mathbf{n}}{}^{k}_{i,j} \mathbf{W}^k_{i,j}) \end{aligned}$$

The horizontal component of the network momentum equation, Equation 22, is dis-

cretized as

$$\frac{\delta_x(\theta_{\delta\mathbf{n}}{}_{i,j}^{k+1}\delta_x\mathbf{V}_{i,j}^{k+1})}{dx^2}+\frac{\delta_y(\theta_{\delta\mathbf{n}}{}_{i,j,}^{k+1}\delta_y\mathbf{V}_{i,j,}^{k+1})}{dy^2} = \frac{\delta_y(\frac{\theta_{\delta\mathbf{n}}{}_{i,j}^{k+1}}{2}\delta_y\mathbf{V}_{i,j}^{k})}{dy^2}-\frac{\delta_y(\frac{\theta_{\delta\mathbf{n}}{}_{i,j}^{k+1}}{2}\delta_x\mathbf{W}_{i,j}^{k})}{dx\ dy} + \frac{\delta_x\Psi(\theta_{\delta\mathbf{n}}{}_{i,j}^{k+1})}{dx}. \quad (24)$$

The equation governing the vertical component of the network velocity has a similar discretization

$$\frac{\delta_x(\theta_{\delta\mathbf{n}}{}_{i,j}^{k+1}\delta_x\mathbf{W}_{i,j}^{k+1})}{dx^2}+\frac{\delta_y(\theta_{\delta\mathbf{n}}{}_{i,j,}^{k+1}\delta_y\mathbf{W}_{i,j,}^{k+1})}{dy^2} = \frac{\delta_x(\frac{\theta_{\delta\mathbf{n}}{}_{i,j}^{k+1}}{2}\delta_x\mathbf{W}_{i,j}^{k})}{dx^2}-\frac{\delta_x(\frac{\theta_{\delta\mathbf{n}}{}_{i,j}^{k+1}}{2}\delta_y\mathbf{V}_{i,j}^{k})}{dx\ dy} + \frac{\delta_y\Psi(\theta_{\delta\mathbf{n}}{}_{i,j}^{k+1})}{dy}. \quad (25)$$

Finally the equation governing the substrate distribution, Equation 18, is discretized as

$$D(\frac{\delta_x((1-\theta_{\delta\mathbf{n}}{}_{i,j}^{k+1})\delta_x\mathbf{c}_{i,j}^{k+1})}{dx^2}+\frac{\delta_y((1-\theta_{\delta\mathbf{n}}{}_{i,j}^{k+1})\delta_y\mathbf{c}_{i,j}^{k+1})}{dy^2}) = g_c(\theta_{\delta\mathbf{n}}{}_{i,j}^{k+1},\mathbf{c}_{i,j}^{k}). \quad (26)$$

The discrete variables also satisfy boundary conditions which are related to those which the continuous variables satisfy. Since all variables are periodic with period L_1, the discretized variables satisfy

$$\begin{aligned}\theta_{\delta\mathbf{n}}(0,y_j,t_k) &= \theta_{\delta\mathbf{n}}(x_N,y_j,t_k)\\ \mathbf{W}(0,y_j,t_k) &= \mathbf{W}(x_N,y_j,t_k)\\ \mathbf{V}(0,y_j,t_k) &= \mathbf{V}(x_N,y_j,t_k)\\ \mathbf{c}(0,y_j,t_k) &= \mathbf{c}(x_N,y_j,t_k)\end{aligned}$$

On Σ_1 and Σ_2 the network satisfies Neumann boundary conditions $\delta_y\theta_{\delta\mathbf{n}}{}_{i,0}^{k}=0$ which implies that $\theta_{\delta\mathbf{n}}{}_{i,-1}^{k}=\theta_{\delta\mathbf{n}}{}_{i,1}^{k}$, where $\theta_{\delta\mathbf{n}}{}_{i,-1}^{k}$ refers to a ghost - point below the numerical domain. Similarly, $\delta_y\theta_{\delta\mathbf{n}}{}_{i,M}^{k}=0$ which implies that $\theta_{\delta\mathbf{n}}{}_{i,M+1}^{k}=\theta_{\delta\mathbf{n}}{}_{i,M-1}^{k}$, where $\theta_{\delta\mathbf{n}}{}_{i,M+1}^{k}$ refers to a ghost - point above the numerical domain. The components of the network velocity are zero on Σ_1 and Σ_2, which implies that $\mathbf{V}_{i,0}^{k}=\mathbf{V}_{i,M}^{k}=0$ and $\mathbf{W}_{i,0}^{k}=\mathbf{W}_{i,M}^{k}=0$.

The discretized substrate satisfies Neumann boundary conditions on Σ_1, hence $\mathbf{c}^k_{i,-1} = \mathbf{c}^k_{i,1}$. The substrate value is fixed at c_{max} on Σ_2, that is $\mathbf{c}^k_{i,M} = c_{max}$.

Then the points on the grid are ordered in (column) lexicographic ordering, which yields matrix equations which are block-tridiagonal. The network equation, (24) can be written as an $(NM \times NM)$ matrix equation, while the flow equations, (24) and (25), yield two $(N(M-2) \times N(M-2))$ matrix equations since the values of the velocities are known on Σ_1 and Σ_2. Likewise since the substrate value is known on Σ_2, the discretized equations can be written as an $(N(M-1) \times N(M-1))$ matrix equation. These four matrix equations are inverted using MATLAB's conjugate-gradient solver.

References

[1] D. G. Allison and M. Goldsbrough, *Polysaccharide production in pseudomonas cepecia*, Journal of Basic Microbiology, 34 (1994), pp. 3–10.

[2] G. Batchelor, *An Introduction to Fluid Dynamics*, Cambridge, U.P., 1967.

[3] R. B. Bird, R. C. Armstrong, and O. Hassager, *Dynamics of Polymeric Liquids*, vol. 1, John Wiley and Sons, New York, 1987.

[4] C.-I. Chen, M. Reinsel, and R. Mueller, *Kinetic investigation of microbial souring in porous media using microbial consortia from oil reservoirs*, Biotechnology and Bioengineering, 44 (1994), pp. 263–269.

[5] J. Dockery and I. Klapper, *Finger formation in biofilm layers*, SIAM Journal on Applied Mathematics, 62 (2002), pp. 853–869.

[6] D. Drew, *Mathematical modeling of two-phase flow*, Annual Reviews of Fluid Mechanics, 15 (1983), pp. 261–291.

[7] H. Eberl, C. Picioreanu, J. Heijnen, and M. van Loosdrecht, *A three dimensional numerical study on the correlation of spatial structure, hydrodynamic conditions, and mass transfer and conversion in biofilms*, Chemical Engineering Science, 55 (2000), pp. 6209–6222.

[8] H. J. Eberl, D. F. Parker, and M. C. V. Loosdrecht, *A new deterministic spatio-temporal continuum model for biofilm development*, Journal of Theoretical Medicine, 3 (2001), pp. 161–175.

[9] H.-C. Flemming and J. Wingender, *Relevance of microbial extracellular polymeric substances (epss) - part i: Structure and ecological aspects*, Water Science and Technology, 43 (2001), pp. 1–8.

[10] ——, *Relevance of microbial extracellular polymeric substances (epss) - part ii: Technical aspects*, Water Science and Technology, 43 (2001), pp. 9–12.

[11] X. He and M. Dembo, *On the mechanics of the first cleavage division of the sea urchin egg*, Experimental Cell Research, 233 (1997), pp. 252–273.

[12] I. Klapper, C. Rupp, R. Cargo, B. Purvedorj, and P. Stoodley, *Viscoelastic fluid description of bacterial biofilm material properties*, Biotechnology and Bioengineering, 80 (2002), pp. 289–296.

[13] R. Kommedal, R. Bakke, J. Dockery, and P. Stoodley, *Modelling production of extracellular polymeric substances in a psuedomonas aeruginosa chemostat culture*, Water Science and Technology, 43 (2001), pp. 129–134.

[14] V. Korstgens, H.-C. Flemming, J. Wingender, and W. Borchard, *Influence of calcium ions on the mechanical properties of a model biofilm mucoid pseudomonas aeruginosa*, Water Science and Technology, 43 (2001), pp. 49–57.

[15] J.-U. Kreft, C. Picioreanu, J. W. T. Wimpenny, and M. C. van Loosdrecht, *Individual-based modelling of biofilms*, Microbiology-SGM, 147 (2001), pp. 2897–2912.

[16] J. U. Kreft and J. Wimpenny, *Effect of eps on biofilm structure and function as revealed by an individual-based model of biofilm growth*, Water Science and Technology, 43 (2001).

[17] A. Kumar and R. K. Gupta, *Fundamentals of Polymers*, The McGraw-Hill Companies inc., New York, 1998, ch. 8 and 9.

[18] R. G. Larson, *The Structure and Rheology of Complex Fluids*, Oxford University Press, New York, 1999.

[19] S. Lubkin and T. Jackson, *Multiphase mechanics of capsule formation in tumors*, Journal of Biomechanical Engineering-Transactions of the ASME, 124 (2002), pp. 237–243.

[20] Y. Osada and K. Kajiwara, eds., *Gels Handbook*, vol. 1, Academic Press, 2001, ch. 1-4.

[21] C. Picioreanu, M. C. van Loosdrecht, and J. J. Heijnan, *Mathematical modeling of biofilm structure with a hybrid differential-discrete cellular automaton approach*, Biotechnology and Bioengeneering, 58 (1998).

[22] ——, *A new combined differential-discrete cellular automaton approach for biofilm modeling: Application for growth in gel beads*, Biotechnology and Bioengeneering, 57 (1998), pp. 718–731.

[23] ——, *Two-dimensional model of biofilm detachment caused by internal stress from liquid flow*, Biotechnology and bioengineering, 72 (2001), pp. 205–218.

[24] C. Picioreanu, M. C. van Loosdrecht, and J. J. Heijnen, *A theoretical study on the effect of surface roughness on mass transportand transformation in biofilms*, Biotechnology and Bioengineering, 68 (2000), pp. 355–369.

[25] P. Saffman and G. Taylor, *The penetration of a fluid into a porous medium or hele-shaw cell containing a more viscous liquid*, Proc. Roy. Soc. A, 245 (1958), pp. 312–344.

[26] H. Tanaka, *Viscoelastic model of phase separation*, Physical Review E, 56 (1997), pp. 4451–4462.

[27] O. Wanner and W. Gujer, *A multispecies biofilm model*, Biotechnology an Bioengineering, 28 (1986), pp. 314–328.

[28] O. Wanner and P. Riechert, *Mathematical modeling of mixed-culture biofilms*, Biotechnology and Bioengineering, 49 (1996), pp. 172–184.

[29] J. Wimpenny and R. Colasanti, *A unifying hypothesis for the structure of microbial biofilms based on cellular automaton models*, FEMS Microb. Ecol, 22 (1997), pp. 1–16.

[30] J. Wingender, T. Neu, and H.-C. Flemming, eds., *Bacterial extracellular polymer substances*, Springer, Heidelberg, Berlin, 1999.

[31] C. Wolgemuth, E. Hoiczyk, D. Kaiser, and G. Oster, *How myxobacteria glide*, Current Biology, 12 (2002), pp. 369–377.

List of Tables

List of Figures